A Polymeric Fastener Can Easily Functionalize Liposome Surfaces with Gadolinium for Enhanced Magnetic Resonance Imaging

Cartney E. Smith,[†] Artem Shkumatov,[†,‡] Sarah G. Withers,[§] Binxia Yang,[§] James F. Glockner,[§] Sanjay Misra,[§] Edward J. Roy,[⊥] Chun-Ho Wong,[∥] Steven C. Zimmerman,[∥] and Hyunjoon Kong[†,‡,*]

[†]Department of Chemical and Biomolecular Engineering, University of Illinois at Urbana—Champaign, 600 South Mathews Avenue, Urbana, Illinois 61801, United States, [‡]Institute for Genomic Biology, University of Illinois at Urbana—Champaign, 1206 West Gregory Drive, Urbana, Illinois 61801, United States, [§]Department of Radiology, Mayo Clinic, 200 First Street SW, Rochester, Minnesota 55905, United States, [⊥]Neuroscience Program and Department of Pathology, University of Illinois at Urbana—Champaign, 506 South Mathews Avenue, Urbana, Illinois 61801, United States, and [∥]Department of Chemistry, University of Illinois at Urbana—Champaign, 600 South Mathews Avenue, Urbana, Illinois 61801, United States

ABSTRACT Common methods of loading magnetic resonance imaging (MRI) contrast agents into nanoparticles often suffer from challenges related to particle formation, complex chemical modification/purification steps, and reduced contrast efficiency. This study presents a simple, yet advanced process to address these issues by loading gadolinium, an MRI contrast agent, exclusively on a liposome surface using a polymeric fastener. The fastener, so named for its ability to physically link the two functional components together, consisted of chitosan substituted with diethylenetriaminepentaacetic acid (DTPA) to chelate gadolinium, as well as octadecyl chains to stabilize the modified chitosan on the liposome surface. The assembly strategy, mimicking the mechanisms by which viruses and proteins naturally anchor to a cell, provided greater T_1 relaxivity than liposomes loaded with gadolinium in both the interior and outer leaflet. Gadolinium-coated liposomes were ultimately evaluated *in vivo* using murine ischemia models to highlight the diagnostic capability of the system. Taken together, this process decouples particle assembly and functionalization and, therefore, has considerable potential to enhance imaging quality while alleviating many of the difficulties associated with multifunctional particle fabrication.

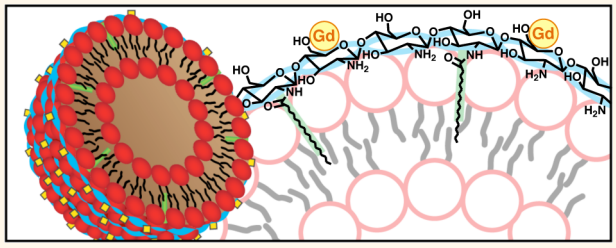

KEYWORDS: MRI · contrast agent · gadolinium · liposome · chitosan · adsorption · relaxivity

Although the clinical use of nanoparticles for the diagnosis or treatment of disease has been under development since the 1960s, a new generation of particles seeks to combine multiple functionalities within a single construct.[1−4] This strategy provides a promising way of noninvasively monitoring biodistribution of therapeutics, while simultaneously treating and tracking disease progression. Additionally, numerous imaging agents may be combined to allow for orthogonal methods of diagnosis in a single dosing.[5−7] Such a method of co-administration is often accomplished by co-encapsulation of multiple components during the fabrication of nano- or microparticles.[8−11] These encapsulation approaches, however, may influence functionality of imaging contrast agents. For example, encapsulating a magnetic resonance imaging (MRI) contrast agent into a particle's interior may limit its interaction with water in surrounding tissues and significantly reduce its relaxivity.[12] Additionally, co-encapsulation of imaging probes and drug molecules may result in undesirable interactions between the two components. Some studies have reported that contrast agents, such as gadolinium chelates, can form noncovalent associations with various proteins, which would have deleterious effects on the efficacy of biomacromolecular therapies.[13−15]

Therefore, efforts are increasingly made to localize imaging contrast agents on

* Address correspondence to hjkong06@illinois.edu.

Received for review January 24, 2013 and accepted October 1, 2013.

Published online October 01, 2013
10.1021/nn4026228

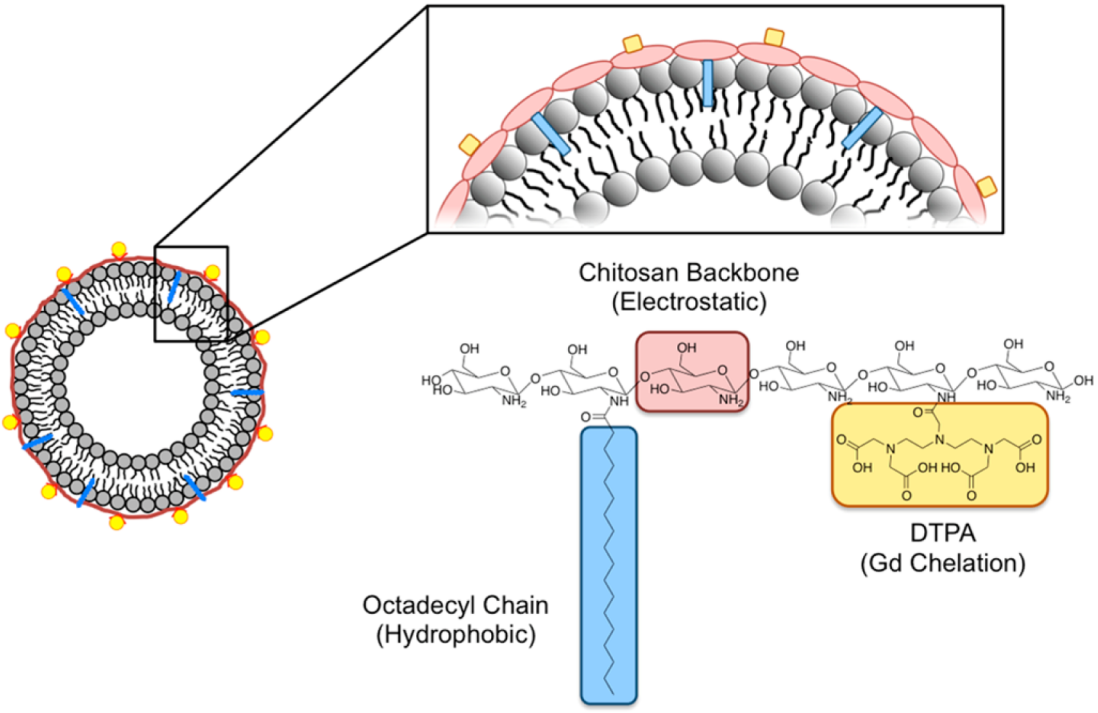

Scheme 1. Schematic diagram of association between a preformed liposome and DTPA−chitosan-g-C_{18}.

particle surfaces. One popular approach is chemical conjugation of micelle-forming molecules or surfactants with contrast agents or their ligands.[16−18] However, these methods may interfere with particle formation and reduce the loading efficiency of drug molecules. Other approaches have therefore focused on chemically modifying the particle surface postfabrication,[19,20] but the accompanying chemical reaction and purification steps raise concerns about the retention and bioactivity of molecules loaded within the carriers.[21] Therefore, there is still a need to exploit an advanced approach that decouples the control of particle assembly from gadolinium loading on the surface, while circumventing concerns regarding additional chemical surface modification steps.

Previously, several biological studies discovered that many biomolecules and pathogens utilize an electrostatic and hydrophobic association to stably associate with a host cell. For example, transmembrane proteins present positively charged amino acid residues and hydrophobic alkyl chains to facilitate association with lipid molecules of a cell membrane.[22−24] Additionally, various viruses associate with cell membranes through similar electrostatic and hydrophobic associations to facilitate intracellular invasion.[25−27] This study presents a strategy to harness these biological interactions in the design of carriers coated with MRI contrast agents using a polymeric fastener. A fastener is defined as a functional unit that physically joins two objects together. In this way, we propose a method to join gadolinium, an MRI contrast agent, with 1,2-dipalmitoyl-*sn*-glycero-3-phosphocholine (DPPC) liposomes as a model carrier. Chitosan conjugated with octadecyl chains and diethylenetriaminepentaacetic acid (DTPA), termed DTPA−chitosan-g-C_{18}, was synthesized as a polymeric fastener to immobilize chelated gadolinium on the liposome surface *via* electrostatic and hydrophobic assembly (Scheme 1). We examined the role of chitosan structure in liposomal surface loading and subsequent enhancement of MRI contrast, as well as the thermodynamics of association between chitosan and liposome using isothermal titration calorimetry (ITC). Outcomes were compared to traditional methods of gadolinium loading, such as encapsulation of gadolinium into the liposome, which have been developed to enhance retention *in vivo*.[28] Overall, the results of this study enable decoupled control of particle assembly and gadolinium loading, offering considerable potential to improve bioimaging quality, as well as to advance the methods used for assembly of multifunctional nano- and microcarriers.

RESULTS AND DISCUSSION

Synthesis and Characterization of DTPA−Chitosan-g-C_{18}. Chitosan capable of binding with both liposome and gadolinium was synthesized by chemically conjugating a controlled number of hydrophobically associating octadecyl chains and gadolinium-binding DTPA to the polymer backbone. The modification of chitosan was performed through a two-step process as depicted in Figure 1a. First, chitosan, consisting of 95.5% deacetylated glucosamine subunits, was conjugated with octadecyl chains through the reaction between the amine groups of chitosan and carbodiimide-activated

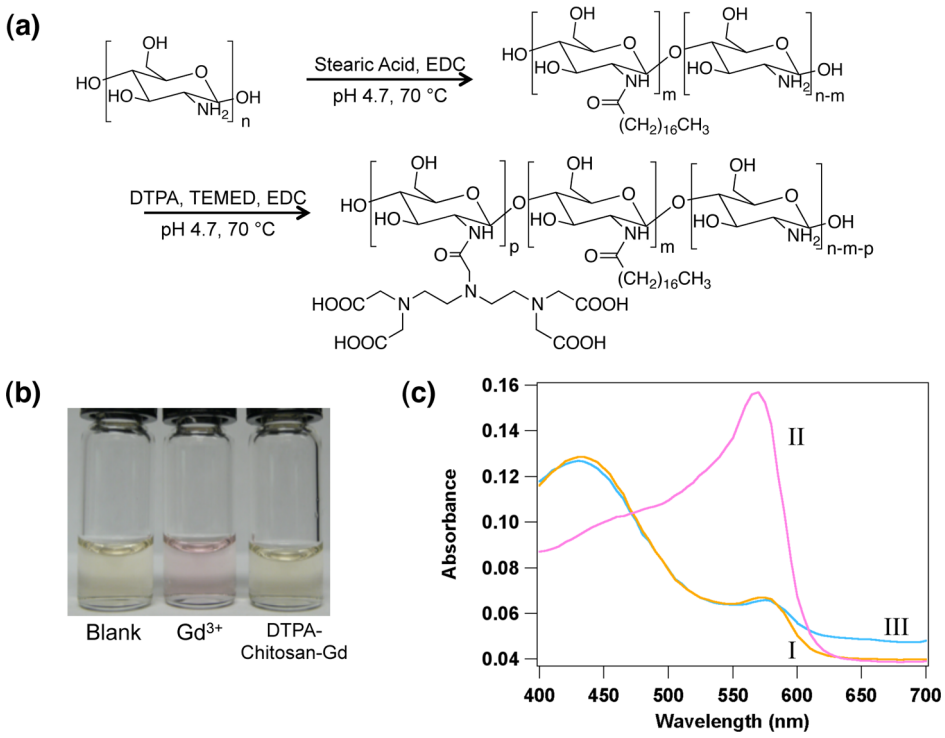

Figure 1. Synthesis and characterization of DTPA−chitosan-g-C_{18}. (a) Synthesis of DTPA−chitosan-g-C_{18} formed by the sequential reaction of stearic acid and DTPA with glucosamine units of chitosan. (b) Color of xylenol orange in media without any $GdCl_3$ (first vial), media with free $GdCl_3$ (second vial), and a mixture of $GdCl_3$ chelated by DTPA−chitosan (third vial). (c) The UV absorbance spectra of xylenol orange in media without $GdCl_3$ (I), media with free $GdCl_3$ (II), and the mixture of $GdCl_3$ chelated by DTPA−chitosan-g-C_{18} (III).

TABLE 1. Characterization of Degree of Substitution of Octadecyl Chains (DS_{C18}) and DTPA (DS_{DTPA}) to Chitosan Using TNBS and Xylenol Orange Assays

stoichiometric DS_{C18} (mol %)	DS_{C18} (mol %)	DS_{DTPA} (mol %)
0		15.3
2	2.3	15.9
5	4.2	15.4

stearic acid.[29] According to the 2,4,6-trinitrobenzene sulfonic acid (TNBS) assay, the degree of substitution of octadecyl chains linked to a chitosan molecule (DS_{C18}) was varied from 0 to 2.3 to 4.2% by altering the molar ratio between stearic acid and glucosamine (see Table 1). The resulting alkyl-substituted chitosan, termed as chitosan-g-C_{18}, remained soluble in water at pH 4.7.

Next, the chitosan-g-C_{18}, as well as unmodified chitosan, was further conjugated with DTPA through the carbodiimide-mediated reaction between amine groups of chitosan and carboxylates of DTPA.[30] The resulting DTPA−chitosan-g-C_{18} was readily dissolved in physiologically relevant and neutral media. Chitosan coupled with DTPA successfully chelated gadolinium, as demonstrated by the retention of yellow color of xylenol orange added to the mixture of DTPA−chitosan-g-C_{18} and $GdCl_3$ (Figure 1b). Note that xylenol orange presents a pink color upon complexation with free gadolinium ions in solution. The active association between DTPA grafted to chitosan and gadolinium was also verified by examining the ratio of absorbance peak heights at 573 and 433 nm[31] (Figure 1c). In the presence of DTPA−chitosan or DTPA−chitosan-g-C_{18}, this ratio did not change as compared to the pure xylenol orange solution. However, without the chelate, there was a dramatic change in the absorbance spectrum, with a 3-fold increase in the ratio of absorbances at 573 and 433 nm. As confirmed by the xylenol orange assay, we could tune the degree of substitution of DTPA to chitosan with the molar ratio between 1-ethyl-3-(3-dimethylaminopropyl)carbodiimide (EDC) and glucosamine unit of chitosan. In this study, the molar ratio between DTPA and EDC was kept constant at 5:1, to circumvent the potential cross-linking reaction between DTPA conjugated to the chitosan molecules. This degree of DTPA substitution was kept constant at approximately 15% for all conditions (Table 1).

Modification of the Liposome Surface Using DTPA−Chitosan-g-C_{18}. Liposomes coated with DTPA−chitosan or DTPA−chitosan-g-C_{18} were prepared by mixing premade liposomes and chitosan molecules in aqueous media. Liposomes with an average diameter of 4.6 ± 2 μm, characterized with phase contrast microscopic images, were first formed by film hydration, and then mixed with DTPA−chitosan or DTPA−chitosan-g-C_{18} with DS_{C18} varied from 2.3 to 4.2% (Figure S1 and Figure 2a).

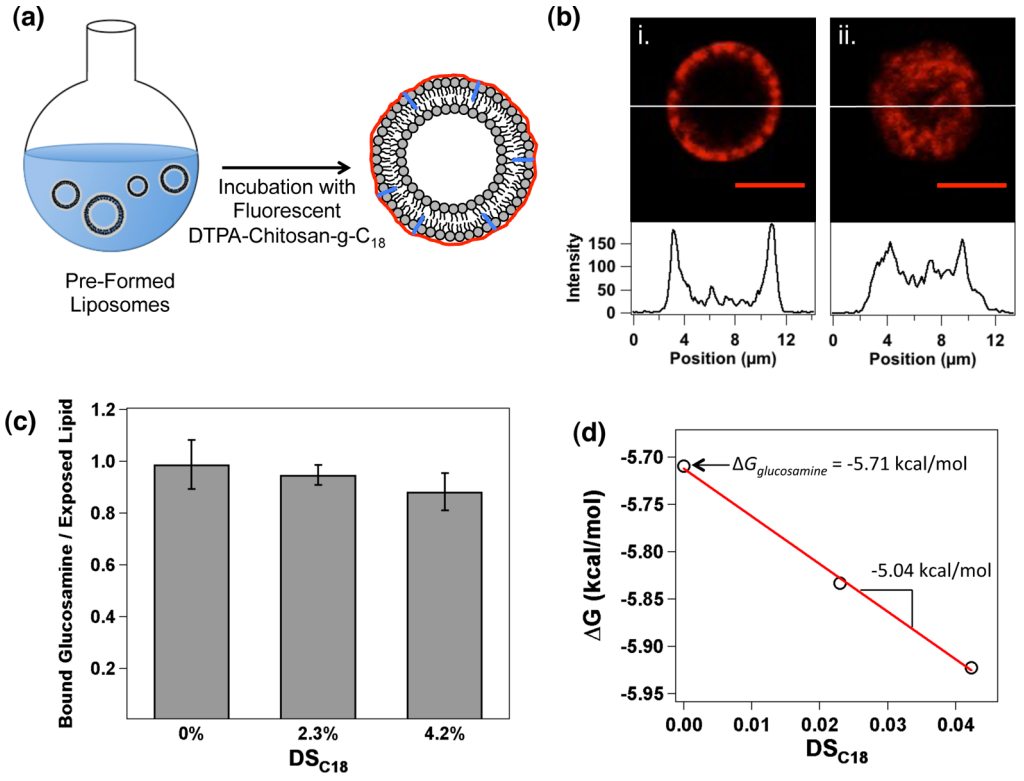

Figure 2. Preparation and analysis of liposomes associated with DTPA−chitosan-g-C_{18} on the outer leaflet. (a) Schematic depicting the process to coat the outer liposome leaflet. (b) A confocal microscopic image of rhodamine-labeled DTPA−chitosan-g-C_{18} anchored to the liposome surface (i), and encapsulated within the liposome (ii). Scale bars represent 5 μm, and intensity profiles are shown across the liposome diameter as indicated. (c) With excess DTPA−chitosan or DTPA−chitosan-g-C_{18}, liposomes were coated at a 1:1 ratio of glucosamine unit to exposed lipid. Therefore, the number of chitosan subunits bound to a liposome was independent of the degree of substitution of octadecyl chains (DS_{C18}). (d) Linear regression of change in Gibbs free energy during the association (ΔG) *versus* DS_{C18}. The *y*-intercept represents the ΔG for a glucosamine unit ($\Delta G_{glucosamine}$), and the slope is equal to the difference between ΔG for octadecyl chains (ΔG_{C18}) and $\Delta G_{glucosamine}$.

The liposome surface was fully saturated with modified chitosan by mixing the two components at a 4:1 molar ratio between glucosamine unit and exposed lipid. To examine the resulting liposome-chitosan association, DTPA−chitosan and DTPA−chitosan-g-C_{18} were labeled with the amine-reactive rhodamine-B isothiocyanate (Figure S2). Within 10 min, the liposome showed positive red fluorescence on its surface, according to cross-sectional images captured with a confocal microscope (Figure 2b). The ring-like appearance of Figure 2b-(i) is in direct contrast to the confocal image of a liposome encapsulating fluorescent DTPA−chitosan-g-C_{18}, formed by hydration of lipids in the presence of the modified chitosan (Figure 2b-(ii)). This visually indicated the surface localization of the chitosan fastener on preformed liposomes. By quantitatively measuring the fluorescent intensity of liposomes after centrifugation, as well as the free chitosan in the supernatant, we found that the number of chitosan molecules bound with the liposome surface was indeed independent of DS_{C18}. These results therefore demonstrate that both DTPA−chitosan and DTPA−chitosan-g-C_{18} readily adsorb onto the liposome surface (Figure 2c). The chitosan associated with liposome remained stable for at least 24 h even after transfer of the liposome particles to chitosan-free phosphate buffered saline (PBS) (results not shown).

However, according to the thermodynamic analysis conducted using ITC, the octadecyl chains grafted to chitosan significantly augmented the association of the chitosan molecules with liposome surface (Figure S3). In this analysis, liposomes were formed by film hydration of DPPC lipids and titrated with solutions of DTPA−chitosan or DTPA−chitosan-g-C_{18} with varied DS_{C18}. Similar to the fluorescence assay presented in Figure 2c, the number of glucosamine units of chitosan bound to the liposome at saturation (*N*) was approximately equal to the number of lipids in the outer leaflet, independent of DS_{C18} (Table 2). In contrast, the equilibrium binding constant, *K*, increased with increasing DS_{C18}. The binding constant is defined as[32]

$$K = \frac{\Theta}{(1-\Theta)C_{free}} \quad (1)$$

where C_{free} is the concentration of unbound glucosamine repeat unit, and Θ is the fraction of exposed

TABLE 2. Thermodynamic Parameters Derived from ITC Analysis of Chitosan−Liposome Binding[a]

DS of C_{18} (mol %)	N	K (10^4 M^{-1})	ΔH (kcal/mol)	ΔG (kcal/mol)	ΔS (cal/mol·K)
0	0.88 ± 0.02	1.55 ± 0.08	2.31 ± 0.07	−5.71	26.9
2.3	0.98 ± 0.05	1.91 ± 0.27	2.43 ± 0.17	−5.83	27.7
4.2	0.89 ± 0.02	2.22 ± 0.12	2.43 ± 0.06	−5.92	28.0

[a] Values are given per mole of glucosamine unit.

lipids bound by modified chitosan. C_{free} is further expanded and related to the total chitosan concentration and saturation binding stoichiometry, N:

$$C_{free} = C_{total} - N\Theta L \quad (2)$$

where L is the concentration of lipids in the outer leaflet of the liposome and assumed to be half of the total lipid concentration. Accordingly, the change in Gibbs free energy (ΔG) of the liposome−chitosan mixture, calculated from K using eq 3, presented negative values for all conditions.

$$\Delta G = -RT\ln(K) \quad (3)$$

These negative values of ΔG indicate that the association of chitosan with liposome is thermodynamically favorable. Interestingly, ΔG decreased linearly with DS_{C18} (Figure 2d).

ΔG was further related to the additive contributions of ΔG for the octadecyl chain (ΔG_{C18}) and ΔG for other glucosamine units ($\Delta G_{glucosamine}$), through eq 4:

$$\begin{aligned}\Delta G &= DS_{C_{18}}(\Delta G_{C_{18}}) + (1 - DS_{C_{18}})(\Delta G_{glucosamine}) \\ &= \Delta G_{glucosamine} + (\Delta G_{C_{18}} - \Delta G_{glucosamine})DS_{C_{18}}\end{aligned} \quad (4)$$

The ΔG_{C18} calculated from the slope and y-intercept of the linear regression curve in Figure 2d is approximately −10.8 kcal/mol. Note that the free energy for transfer of a hydrocarbon chain into a micelle or bilayer has previously been reported as approximately −0.7 kcal/mol per methylene group.[33] Therefore, it is suggested that most methylene units of the octadecyl chain grafted to chitosan are inserted into the liposome bilayer *via* hydrophobic assembly, thus further stabilizing DTPA−chitosan-g-C_{18} on the liposome surface.

Changes in enthalpy, (ΔH), were calculated by relating it to the total heat of the solution (Q) measured with ITC, as shown in eq 5

$$Q = N\Theta V_0 L\Delta H \quad (5)$$

where V_0 is the total volume of the sample cell. In all cases, ΔH was positive, which suggests that the association between liposome and chitosan was endothermic for all conditions. This result is similar to previous studies for the association of unmodified chitosan with zwitterionic lipids.[34] Additionally, the change in entropy (ΔS), calculated from ΔH and ΔG using eq 6 also presented positive values for all conditions.

$$\Delta S = \frac{\Delta H - \Delta G}{T} \quad (6)$$

Interestingly, ΔS increased with DS_{C18} of DTPA−chitosan-g-C_{18} (Table 2).

Taken together, we interpret that the increase in entropy is responsible for the thermodynamically favorable association between liposome and modified chitosan molecules. The positive ΔS is likely due to the release of counterions and water molecules bound with chitosan and liposome surfaces, as electrostatic interactions are established between charged chitosan subunits and exposed lipids. It is also likely that the octadecyl chains grafted to chitosan molecules confer an additional increase in ΔS with increasing DS_{C18} of DTPA−chitosan-g-C_{18} due to desolvation upon insertion into the bilayer. These different association mechanisms and thermodynamic contributions between DTPA−chitosan and DTPA−chitosan-g-C_{18} significantly influenced the amount of gadolinium loaded on the liposome surface, as will be demonstrated in the subsequent section.

Loading Gadolinium on a Liposome Surface. As expected, liposomes associated with either DTPA−chitosan or DTPA−chitosan-g-C_{18} of varying DS_{C18} could immobilize gadolinium on their surfaces. In this study, coated liposome particles were mixed with $GdCl_3$ to saturate the conjugated DTPA (Figure 3a). Complete chelation was verified by the xylenol orange assay. Liposomes coated by DTPA-modified chitosan were able to associate with gadolinium and produce the same spectrum as pure xylenol orange solution (Figure 3b). Conversely, in the absence of chitosan, bare liposomes mixed with gadolinium showed a 3-fold increase in the ratio of absorbances at 573 and 433 nm. These results clearly confirm that gadolinium is stably immobilized on the liposome surface through the adsorption of DTPA−chitosan or DTPA−chitosan-g-C_{18}.

Interestingly, however, the amount of gadolinium immobilized on the liposome surface was significantly dependent on whether the DTPA−chitosan was modified by octadecyl chains. According to the quantitative fluorescence assay to determine the number of rhodamine-labeled chitosan molecules remaining on the liposome surface after addition of $GdCl_3$, complexation of gadolinium with DTPA triggered 30% of the DTPA−chitosan to desorb from the liposome surface (Figure 3c). In contrast, DTPA−chitosan-g-C_{18} showed minimal desorption. Therefore, as a result, the gadolinium surface loading was approximately 1.4 times larger with DTPA−chitosan-g-C_{18}. These results suggest that the gadolinium bound to DTPA−chitosan destabilize the electrostatic association between chitosan molecules and liposome surface. In contrast, octadecyl chains of the DTPA−chitosan-g-C_{18}, which hydrophobically associated with alkyl chains of lipid

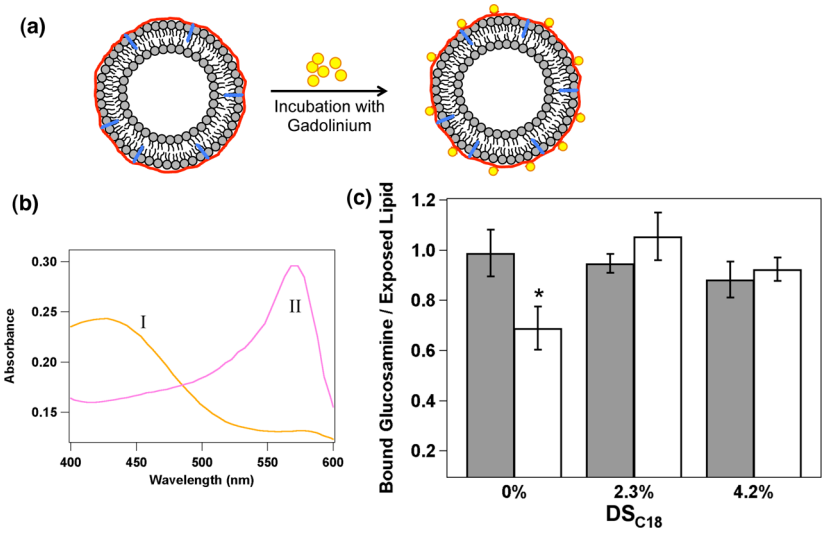

Figure 3. Gadolinium loading on the liposome surface *via* DTPA−chitosan or DTPA−chitosan-g-C_{18}. (a) Schematic depicting gadolinium chelation by chitosan-coated liposomes. (b) The xylenol orange absorbance spectra of the mixture of $GdCl_3$ and liposome coated by DTPA−chitosan or DTPA−chitosan-g-C_{18} (I) and the mixture of $GdCl_3$ and uncoated liposome (II). (c) Analysis of DTPA−chitosan or DTPA−chitosan-g-C_{18} bound to a liposome with (open bars) and without (shaded bars) addition of $GdCl_3$ in the liposome suspension. Asterisk (*) represents statistical significance of the difference in the amount of DTPA−chitosan adsorbed to liposomes in the presence and absence of $GdCl_3$ (*$p < 0.05$).

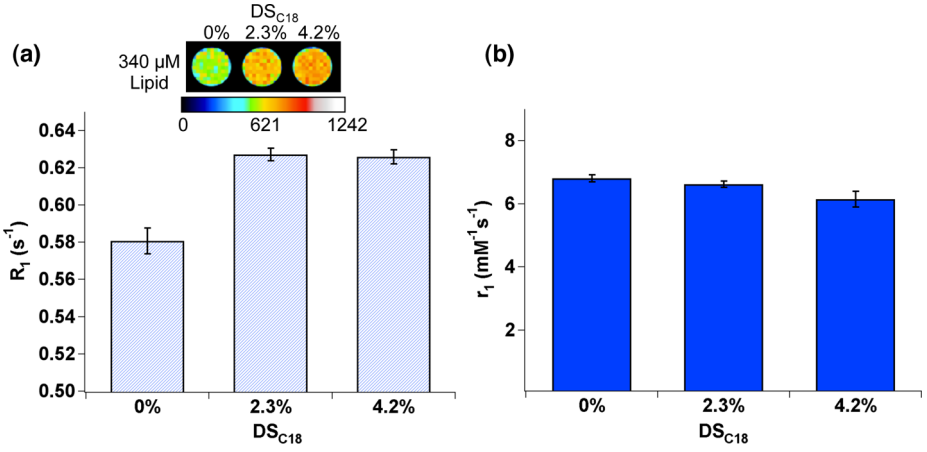

Figure 4. Effects of DS_{C18} of DTPA−chitosan-g-C_{18} on the liposome's ability to enhance MRI contrast. (a) Pseudocolored MR phantom image and longitudinal relaxation rate (R_1) of the gadolinium-loaded liposome (TI = 1000 ms). MR contrast and R_1 were further increased with liposomes coated by DTPA−chitosan-g-C_{18}. The scale bar represents MR signal intensity. (b) The independence of molar relaxivity (r_1) on DS_{C18}. Error bars represent standard deviation of the fit parameter.

molecules, likely act as an anchor to mitigate the tendency of gadolinium to electrostatically separate chitosan from the liposome surface.

Evaluation of Gadolinium-Loaded Liposome Contrast Capability. The ability of gadolinium-loaded liposomes to enhance MRI contrast was evaluated using a 3 T clinical MRI scanner. MR phantom images were acquired using an inversion recovery turbo spin echo (IR-TSE) pulse sequence to evaluate spin−lattice relaxation time (T_1). Molar relaxivity was then determined by linear regression of the longitudinal relaxation rate ($R_1 = 1/T_1$) *versus* gadolinium concentration. Gadolinium loaded on the liposome modified by DTPA−chitosan-g-C_{18} significantly enhanced MR signal, compared to the liposome modified with DTPA−chitosan (Figure 4a). At a given liposome concentration, R_1 of the suspension was increased with DTPA−chitosan-g-C_{18}. However, the molar relaxivity of immobilized gadolinium was nearly the same across samples, regardless of DS_{C18} (Figure S4 and Figure 4b). Therefore, we interpret that the enhancement of R_1 attained with DTPA−chitosan-g-C_{18} is due solely to the higher loading of gadolinium on the liposome surface, noting that 30% of the DTPA−chitosan was desorbed upon exposure to $GdCl_3$ as shown in Figure 3c.

Additionally, at a given gadolinium concentration, the gadolinium-loaded liposomes assembled through sequential addition of DTPA−chitosan-g-C_{18} and $GdCl_3$ to preformed vesicles enhanced MR signal more significantly than gadolinium encapsulated *in situ* during

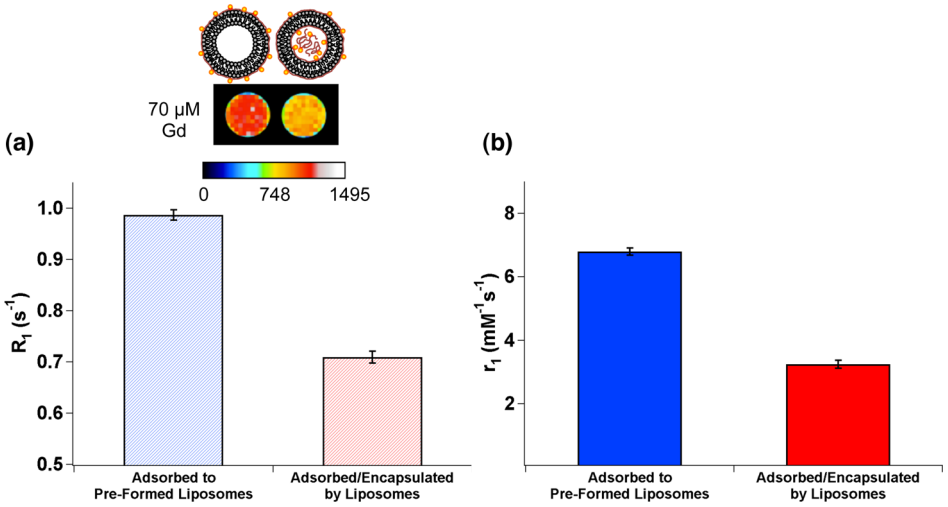

Figure 5. Effects of gadolinium loading strategy on MR signal and molar relaxivity of gadolinium. (a) Pseudocolored MR phantom image and longitudinal relaxation rate (R_1) of liposomes bound with gadolinium exclusively on the outer leaflet (left liposome in the MR image) and on both outer leaflet and interior of the liposome (right liposome in the MR image), (TI = 1000 ms). The total gadolinium concentration in the phantom samples was kept constant at 70 μM. (b) Molar relaxivities (r_1) of the liposomes bound with gadolinium on the outer leaflet (blue bar) and liposomes with gadolinium adsorbed on the exterior and encapsulated (red bar). Error bars represent standard deviation of the fit parameter.

liposome formation. In the analysis shown in Figure 5a, the gadolinium concentration was kept constant at 70 μM for both two conditions according to ICP-OES analysis. Noting that the amount of gadolinium per liposome was greater in the case of loading both in the interior and on the surface as compared to surface loading only, the number of liposomes per MR phantom sample was greater for liposomes loading gadolinium on their surfaces. Interestingly, the longitudinal relaxation rate (R_1) and the corresponding signal intensity of the phantom made with gadolinium localized on the outer leaflet were significantly greater than that made by encapsulation. This can be attributed to the greater total number of gadolinium ions anchored to the liposome surface. As such, the molar relaxivity of surface-bound gadolinium was twice that of gadolinium incorporated *via in situ* encapsulation (Figure 5b).

This boost in relaxivity, and subsequent MR signal enhancement, are likely derived from enhanced contact with free water in surrounding media, in contrast to the limited interaction available to gadolinium within the liposome interior. Therefore, these results systematically rationalize the necessity to load gadolinium exclusively on particle surfaces for enhancing MR images. Furthermore, the relaxivity was enhanced beyond that of the clinically used unconjugated DTPA–gadolinium complex with a molar relaxivity of 4.85 mM^{-1} s^{-1} (Figure S3).

Stability Analysis of Gadolinium-Loaded Liposomes in Serum-Supplemented Media. We further analyzed the stability of the association between DTPA–chitosan-g-C_{18} and liposome surfaces by incubating the liposome particles in media supplemented with 10% human serum at 37 °C, which is conventionally used to assess structural stability of nanoparticle formulations. Stability was monitored over the course of an hour to match the *in vivo* incubation period presented in the following sections. According to measurements of fluorescence intensity from liposomes after centrifugation to remove free chitosan molecules, more than 60% of the initially adsorbed DTPA–chitosan-g-C_{18} remained on the liposome surface (Figure S5). We interpret that the desorption of chitosan from liposomes may result in part from the intrinsic instability of liposome particles in circulation, as characterized by an increase in liposome permeability and structural disintegration.[35,36] We therefore propose that further optimization of the liposome itself to enhance stability in future studies would minimize the loss of DTPA–chitosan-g-C_{18} from the liposome surface. Additionally, the liposomes did not aggregate over the course of one-hour incubation according to optical images, and the average diameter changed minimally (Figure S6). However, there was an observable reduction in the number of liposomes following incubation in the serum-supplemented media.

Despite detachment, DTPA–chitosan-g-C_{18} was able to retain its association with gadolinium in the presence of serum. The resulting complex of gadolinium and DTPA–chitosan-g-C_{18} was minimally toxic to cells, as evaluated with an MTT assay widely used to evaluate cytotoxicity. Endothelial cells incubated with gadolinium loaded on the liposome surface, as well as those incubated with gadolinium bound to free DTPA–chitosan-g-C_{18}, retained their metabolic activity, similar to untreated cells (Figure S7). In contrast, half of the cells incubated with unchelated gadolinium over 24 h were no longer metabolically active.

***In Vivo* Performance of Gadolinium-Loaded Liposomes.** To evaluate the capability of the gadolinium-coated

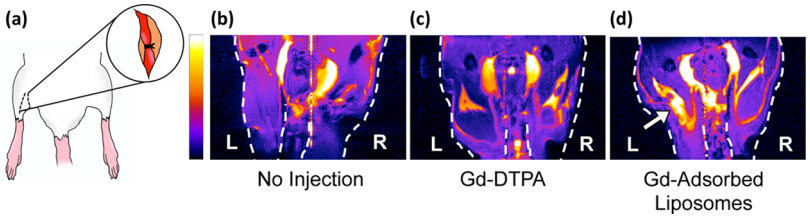

Figure 6. Evaluation of gadolinium contrast agents with a murine model of hindlimb ischemia. (a) The femoral artery of the left hindlimb was ligated to prevent blood flow. (b–d) MR images of left and right hindlimbs of (b) a mouse that did not receive gadolinium, (c) a mouse that was injected with DPTA–gadolinium chelates, and (d) a mouse injected with gadolinium loaded on liposome surfaces. The arrow in (d) indicates significant accumulation of liposomes loaded with gadolinium. The color scale bar is proportional to MR signal intensity, and images are presented at the same grayscale levels.

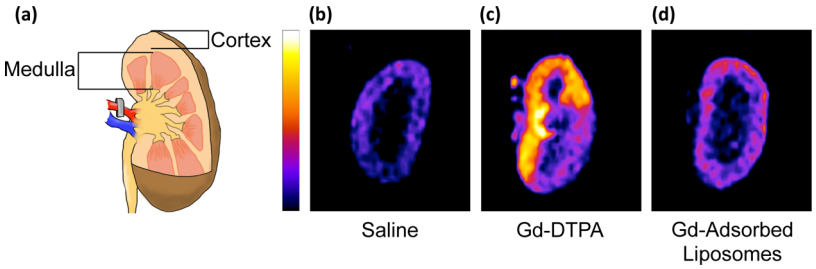

Figure 7. Analysis of gadolinium-loaded liposomes in a rat model of renal ischemia. (a) Renal arteries were occluded prior to injection of contrast agent. (b–d) MR images of coronal sections of kidneys injected with (b) saline, (c) free gadolinium–DTPA, and (d) liposomes surface-loaded with gadolinium. Images are pseudocolored and shown on the same grayscale.

liposomes to highlight target tissues of interest *in vivo*, two separate animal experiments were conducted using murine models with occlusive blood flow in femoral or renal arteries. First, an ischemic injury was induced in the left hindlimb of male BALB/c mice using a suture to occlude the femoral artery.[37] Such a model is often used to study peripheral vascular diseases that result in reduced or blocked blood flow to limbs, and ultimately limb infarction if not diagnosed and treated early. These vascular defects are caused by vascular occlusion, rupture, or leakage, characteristic of atherosclerosis, vascular leak syndrome, and other cardiovascular diseases.[38,39] Through the tail vein, mice were either injected with gadolinium loaded on liposome surfaces using DTPA–chitosan-g-C_{18} (DS_{C18} = 4.2%), or with unconjugated DTPA–gadolinium, as a control. The dosage of gadolinium was kept constant at 0.04 mmol/kg.

One hour after injection, mice were imaged with a 14.1 T MR scanner to examine whether the injected liposome particles could enhance imaging of the occluded artery. Based on serum stability studies, we expected gadolinium would sufficiently remain on the liposome surfaces over the course of the experiment. In comparison to a mouse that received the ischemic injury but no injection of gadolinium, both the liposome-bound and free gadolinium chelates provided signal enhancement in the hindlimbs (Figure 6). However, only in the case of gadolinium loaded on the liposome surface, the occluded artery was illustrated by greater area and intensity of the highlighted region than that of the uninjured right hindlimb. We therefore suggest that the liposomes were better able to accumulate in the occluded area than free DTPA–gadolinium. In this way, the gadolinium adsorbed to the liposome surface could locally enhance the relaxation rate in the extravascular tissue and subsequently provide contrast. Such discrimination between ischemic and nonischemic limbs was not observed with the free DTPA–gadolinium, which emphasized the advantage of binding gadolinium to the liposome surface in the diagnosis of peripheral vascular diseases.

To further underscore the applicability of gadolinium-adsorbed liposomes *in vivo*, the system was administered in a rat model of renal ischemic injury. MR imaging is commonly used to diagnose renal diseases based on changes in anatomical structure, however, the use of gadolinium-based contrast agents may be limited due to lack of corticomedullary differentiation.[40] A major reason for this is the rapid transport of small gadolinium chelates from cortex to medulla during renal excretion.

First, renal arteries were clamped for 45 min to induce an ischemic state in the kidney. Saline, gadolinium in the form of free DTPA chelate, or gadolinium anchored to liposomes was injected into the left kidney through the renal artery. Five minutes after injection, kidneys displayed enhanced signal compared to the saline-injected control (Figure 7). However, in the case of the kidney injected with free DTPA chelate, medulla was not as readily delineated from cortex, as expected. The contrast agent appeared unevenly distributed throughout the kidney. Conversely, the gadolinium-loaded liposomes were localized within the cortex and

were able to clearly differentiate cortex from medulla, as confirmed by near-infrared (NIR) fluorescence images of liposomes labeled with CellVue NIR815 dye. (Figure S8).

These results clearly underscore the utility of DTPA–chitosan-g-C_{18} in imbuing a liposome with MRI contrast capabilities due to (1) the higher loading of gadolinium on the liposome surface provided by hydrophobic stabilization and (2) enhanced molar relaxivity through surface localization. We envision that the contrast enhancement provided by this fabrication strategy can be further improved by modifying the chemical structure of DTPA–chitosan-g-C_{18}. For example, coating of the liposome surface with chitosan-g-C_{18} substituted with a greater amount of DTPA would significantly increase gadolinium loading on the liposome and heighten the liposome's ability to increase MR contrast.

Additionally, this process facilitates separation of secondary imaging contrast agents or drug molecules from gadolinium by incorporating them inside the liposome, so as to circumvent potential interaction between gadolinium and other functional molecules. Moreover, we propose that this process has benefits beyond MRI. For example, chitosan-g-C_{18} could be modified with peptides capable of binding with target pathological tissues. This strategy represents another way in which the efficiency of the functional unit is improved when localized on the liposome surface. Furthermore, though chitosan has been shown to demonstrate stealth properties in some cases,[41,42] the chitosan fastener may be further modified with poly(ethylene glycol) to reduce potential opsonization and enhance *in vivo* retention. Separately, the liposome composition and particle size may be optimized for the particular application. Overall, our process of coating liposomes postfabrication with the chitosan fastener should be advantageous to decoupling the particle assembly from the particle surface modification for independent tunability of functional units.

CONCLUSION

Overall, this study demonstrates a simple, yet unreported method to functionalize liposome surfaces with gadolinium, an MRI contrast agent, using DTPA–chitosan-g-C_{18}. Upon mixing premade liposomes with the DTPA–chitosan-g-C_{18} fastener, octadecyl chains were inserted into the lipid membrane *via* hydrophobic association, as confirmed by ITC. Subsequently, the octadecyl chains minimized desorption of chitosan molecules from the liposome triggered by chelation of gadolinium with DTPA. Therefore, liposomes loaded with gadolinium on their surfaces *via* DTPA–chitosan-g-C_{18} displayed a greater capacity to enhance MR contrast than liposomes modified by alkyl-free DTPA–chitosan. Additionally, this sequential assembly process to localize gadolinium on the exterior of the liposome greatly enhanced the molar relaxivity of gadolinium and subsequently MRI contrast, as compared to methods that incorporate gadolinium inside the liposome. Using *in vivo* models, we were also able to demonstrate the utility of the gadolinium-loaded liposomes in detecting and imaging ischemic sites. Taken together, this assembly strategy using a chitosan fastener will be broadly useful not only for functionalizing liposome surfaces with a wide array of imaging, targeting, and therapeutic modalities, and but also for spatially organizing them.

EXPERIMENTAL SECTION

Synthesis of DTPA–Chitosan-g-C_{18}. Chitosan (Sigma-Aldrich) was dissolved in a 50 mM aqueous HCl solution heated to 70 °C. Additional HCl was added to adjust the pH to 4.7 after chitosan was completely dissolved. Separately, varying amounts of stearic acid (Sigma-Aldrich)—2% or 5% with respect to glucosamine repeat unit of chitosan—were dissolved in ethanol at 70 °C. After dissolution of stearic acid, the solution was brought to room temperature and 1-ethyl-3-(3-dimethylaminopropyl) carbodiimide (EDC, Sigma-Aldrich) was added at a molar ratio of 5:1 EDC to stearic acid. The stearic acid/EDC solution was then added to the dissolved chitosan and reacted at 70 °C. The volume ratio between ethanol and HCl solution was kept constant at 1:2 for all conditions. After 24 h, the temperature was gradually reduced to room temperature, and the mixture continued to stir for another 24 h.

Then, ethanol was removed by precipitation in NaOH and the chitosan-g-C_{18} was resuspended in HCl. Briefly, 50 mM NaOH was added to the solution of chitosan-g-C_{18}, followed by centrifugation for 10 min at 4000 rpm. The supernatant was removed, and the precipitate was redissolved in 50 mM HCl aqueous solution at 70 °C. This precipitation/dissolution process was repeated twice to ensure removal of ethanol.

Next, diethylenetriaminepentaacetic acid (DTPA, Sigma-Aldrich) was dissolved in deionized water. Tetramethylethylenediamine (TEMED, Sigma-Aldrich) was added to the DTPA solution to adjust the pH of the mixture to 4.7. The DTPA solution was then further mixed with EDC dissolved in 50 mM HCl aqueous solution. The molar ratio between DTPA and EDC was kept constant at 5:1, to minimize cross-linking between glucosamine units of chitosan and the multiple carboxylate groups of DTPA. The DTPA/EDC mixture was finally added to the chitosan or chitosan-g-C_{18} solutions and allowed to react for 24 h at 70 °C, followed by another 24 h at room temperature. The resulting DTPA–chitosan and DTPA–chitosan-g-C_{18} were purified by dialysis (MWCO 6000–8000 regenerated cellulose tubing, Fisher Scientific) against 0.1 M NaCl for two days. The product was then further dialyzed in deionized water for one day. The purified product was then lyophilized, and kept in powder form before use.

Characterization of DTPA–Chitosan and DTPA–Chitosan-g-C_{18}. The degree of substitution of octadecyl chains to chitosan was determined by a 2,4,6-trinitrobenzene sulfonic acid (TNBS, Sigma-Aldrich) assay, which quantifies the amount of unreacted amines on chitosan. Briefly, modified chitosan samples were dissolved in an 0.1 M acetate buffer at pH 5.0 and mixed with 0.1% (w/v) TNBS at 37 °C. After incubation for 5 h, the absorbance of each mixture was measured at 335 nm with a microplate reader (Tecan Infinite 200 PRO, Tecan AG, Switzerland).

The degree of substitution of DTPA grafted to chitosan was quantified by the xylenol orange assay. A $GdCl_3$ ($GdCl_3 \cdot 6H_2O$,

Sigma-Aldrich) solution was added incrementally to a solution of DTPA–chitosan or DTPA–chitosan-g-C_{18}. After each addition, an aliquot was mixed with xylenol orange tetrasodium salt (Sigma Aldrich) in acetate buffer (50 mM, pH 5.80) to determine whether any gadolinium remained unchelated, as indicated by a change in the ratio of the absorbances at 573 and 433 nm. The amount of gadolinium required to cause a change in the absorbance ratio was used to calculate the DS of DTPA.

Liposome Preparation. Liposomes were prepared by a film hydration method followed by sonication. 1,2-Dipalmitoyl-*sn*-glycero-3-phosphocholine (Avanti Polar Lipids) was dissolved in chloroform (Fisher Scientific) and placed in a round-bottom flask. Chloroform was removed by rotary evaporation to yield an evenly distributed film. The film was then hydrated with deionized water at 50 °C, which is above the transition temperature of DPPC. The lipid concentration was kept constant at 1 mg/mL. Following hydration, liposome suspension was placed on an ice bath and sonicated for 15 min. For experiments involving *in situ* encapsulation of gadolinium and DTPA–chitosan-g-C_{18} in the liposome, DTPA–chitosan-g-C_{18} was first complexed with $GdCl_3$. The lipid film, formed as described above, was then hydrated with the aqueous mixture of gadolinium and DTPA–chitosan-g-C_{18}.

Analysis of Chitosan on the Liposome Surface. To quantitate the association between modified chitosans and liposomes, chitosan molecules were first labeled with rhodamine. DTPA–chitosan or DTPA–chitosan-g-C_{18} were dissolved in neutral deionized water and reacted overnight with rhodamine-B isothiocyanate (Sigma-Aldrich), in which the isothiocyanate functional moiety reacted with the primary amine groups of the chitosan backbone (Figure S2). Then, chitosan solutions were dialyzed against 0.1 M NaCl solution followed by deionized water to remove any unreacted rhodamine. Finally, the labeled chitosan molecules were lyophilized and kept dried until use. The rhodamine-labeled chitosans were adsorbed to preformed liposomes by stirring them together at room temperature for 10 min or 12 h, followed by centrifugation at 4000 rpm for 10 min. The supernatant, containing excess chitosan molecules, was then removed, and the pelleted liposomes were resuspended in deionized water. Concentrations of rhodamine-labeled chitosan in supernatant and resuspended liposome were analyzed by exciting the samples at 535 nm and measuring fluorescence intensity at 595 nm using a microplate reader (Tecan Infinite 200 PRO, Tecan AG, Switzerland). A standard curve was developed by serial dilution of the chitosan/liposome solution prior to centrifugation. For analysis, four replicates were prepared for each condition. Statistical significance between each sample set was determined from a two-tailed, unpaired Student's *t* test in Microsoft Excel, in which differences were considered significant for $p < 0.05$. Additionally, chitosan adsorption onto liposomes was visualized using a laser scanning confocal microscope (LSM 700, Carl Zeiss Microimaging, GmbH, Germany).

Loading and Analysis of Gadolinium on the Liposome Surface. A 7.56 mM $GdCl_3$ solution was added to the aqueous suspension of liposomes modified by DTPA–chitosan or DTPA–chitosan-g-C_{18} at a 1:1 ratio of gadolinium to DTPA. Complete chelation was verified by xylenol orange assay. To quantify the amount of modified chitosan adsorbed to the liposome after gadolinium addition, fluorescently labeled DTPA–chitosan and DTPA–chitosan-g-C_{18} were used as described in the previous section. After incubation with gadolinium for 12 h, samples were centrifuged for 10 min at 4000 rpm. The concentrations of chitosan in both supernatant and resuspended liposomes were determined using the Tecan Infinite 200 PRO microplate reader as described. Again, four replicates were made per condition and analyzed for significance using a two-tailed, unpaired Student's *t* test.

Thermodynamic Analysis of Association between Chitosan and Liposome by Isothermal Titration Calorimetry. Isothermal titration calorimetry (ITC) analysis was performed at 25 °C with a MicroCal VP-ITC calorimeter (MicroCal, Northampton, MA). The 1.45 mL sample cell was filled with an aqueous liposome suspension at a total lipid concentration of 0.4 mM. The cell was titrated with 28 injections of 10 μL chitosan solution (5 mM glucosamine unit concentration). Each injection was performed over 17.1 s with a delay of 300 s between injections while stirring at 310 rpm. Data analysis was performed with Origin 5.0 software from MicroCal to yield thermodynamic binding parameters such as the binding constant, change in enthalpy, and change in entropy by fitting data to a single-site binding model.[32] The first data point was not included in the analysis.

T_1 Relaxivity Measurements. Measurements and imaging of MRI phantoms were performed with a head coil on a 3 T Siemens Magnetom Allegra MR scanner (Siemens AG, Erlangen, Germany). Images were produced with an inversion recovery turbo spin echo (IR-TSE) pulse sequence. The sequence used a repetition time (TR) of 2500 ms and an echo time (TE) of 10 ms. The inversion time (TI) was varied from 100 to 1700 ms to determine T_1 by nonlinear least-squares curve fitting to eq 7:

$$S(\mathrm{TI}) = S_0[1 - (1 - k)e^{-\mathrm{TI}/T_1}] \quad (7)$$

where S(TI) is the signal intensity measured by ImageJ software, S_0 is the signal at thermal equilibrium, and k is a constant related to the flip angle and magnetization of the system.[43] Relaxation rate, R_1 was then calculated as the inverse of relaxation time ($1/T_1$).

Longitudinal relaxivity, r_1, was found by linear regression of the plot of R_1 *versus* gadolinium concentration according to eq 8:

$$1/T_1 = 1/T_{1,\mathrm{water}} + r_1[\mathrm{Gd}] \quad (8)$$

where $T_{1,\mathrm{water}}$ is the longitudinal relaxation time of gadolinium-free media and [Gd] is the total gadolinium concentration within a sample. For these measurements, gadolinium concentration was determined by inductively coupled plasma optical emission spectroscopy (ICP-OES, Perkin-Elmer Optima 2000 DV, Norwalk, CT) after digestion of samples in a concentrated nitric acid solution.

Assessment of Gadolinium-Loaded Liposome Using a Hindlimb Ischemia Model. The surgery to induce hindlimb ischemia was performed in accordance with the protocol approved by the Illinois Institutional Animal Care and Use Committee. The mice used were male BALB/c mice (Jackson Laboratories, ME) weighing approximately 30 g. Prior to surgery, mice were anesthetized with an intraperitoneal injection of a xylazine (10 mg/kg) and ketamine hydrochloride (100 mg/kg) cocktail. Hair was removed from the left hindlimb and a small incision was made on the upper thigh to expose the femoral artery and vein. The artery and vein were then ligated with 5–0 Ethilon sutures (Johnson & Johnson, NJ) to prevent blood flow to the limb. For mice receiving injection, 0.04 mmol/kg of gadolinium was then administered *via* tail vein.

Mice were imaged 1 h after injection with a 14.1 T Varian microimager consisting of a Unity/Inova 600 MHz NMR spectrometer (Varian, CA) equipped with a custom-made adjustable radio frequency coil.[44] T_1-weighted Coronal images of the mouse hindlimbs were acquired using a spin–echo multislice (SEMS) pulse sequence with the following parameters: slice thickness, 0.5 mm; TR, 350 ms; TE, 10 ms; matrix size, 256 × 256.

Evaluation of Gadolinium-Loaded Liposome Using a Renal Ischemia Model. Procedures to induce renal ischemia were carried out according to the protocol approved by the Mayo Clinic Institutional Animal Care and Use Committee. The rats used were Sprague–Dawley rats (Jackson Laboratories, ME) weighing 300–400 g. Rats were anesthetized *via* intraperitoneal injection of xylazine (20 mg/kg) and ketamine hydrochloride (200 mg/kg). Anesthesia was maintained with intraperitoneal pentobarbital (20–40 mg/kg). An abdominal incision was then made and the renal arteries were clamped bilaterally for 45 min. Kidneys were then injected *via* the renal artery with gadolinium–DTPA, liposomes loaded with gadolinium *via* DTPA–chitosan-g-C_{18} (DS_{C18} = 4.2%), or saline. Kidneys injected with contrast agent received gadolinium doses of 0.3 μmol. Five minutes after injection, kidneys were removed for MR imaging.

Images were acquired with a 3 T Siemens MR scanner (AG, Erlangen, Germany). A three-dimensional spoiled gradient recalled (3D SPGR) sequence produced T_1-weighted images using

the following parameters: slice thickness, 2 mm; TR, 7.3 ms; TE, 3.2 ms; flip angle, 15°; matrix size 352 × 224.

Conflict of Interest: The authors declare no competing financial interest.

Supporting Information Available: Optical image of liposomes, reaction scheme for fluorescent labeling, ITC thermograms, relaxivity plots, serum stability testing, cytotoxicity evaluation, and fluorescent imaging of kidney cross sections. This material is available free of charge *via* the Internet at http://pubs.acs.org.

Acknowledgment. This work was supported by the National Institutes of Health (1R01 HL109192 to H.J.K., S.M., and S.C.Z., R01 HL098967 to S.M., and Chemistry-Biology Interface Training Grant 5T32-GM070421 to C.E.S.) and The Center for Advanced Study at the University of Illinois. We also thank B. Odintsov and R. Larsen at the Beckman Institute for Advanced Science and Technology in the University of Illinois at Urbana—Champaign for assistance with MR imaging.

REFERENCES AND NOTES

1. Jokerst, J. V.; Gambhir, S. S. Molecular Imaging with Theranostic Nanoparticles. *Acc. Chem. Res.* **2011**, *44*, 1050–1060.
2. Shi, J.; Xiao, Z.; Kamaly, N.; Farokhzad, O. C. Self-Assembled Targeted Nanoparticles: Evolution of Technologies and Bench to Bedside Translation. *Acc. Chem. Res.* **2011**, *44*, 1123–1134.
3. Gianella, A.; Jarzyna, P. A.; Mani, V.; Ramachandran, S.; Calcagno, C.; Tang, J.; Kann, B.; Dijk, W. J. R.; Thijssen, V. L.; Griffioen, A. W.; *et al.* Multifunctional Nanoemulsion Platform for Imaging Guided Therapy Evaluated in Experimental Cancer. *ACS Nano* **2011**, *5*, 4422–4433.
4. Lavik, E.; von Recum, H. The Role of Nanomaterials in Translational Medicine. *ACS Nano* **2011**, *5*, 3419–3424.
5. Weissleder, R.; Pittet, M. J. Imaging in the Era of Molecular Oncology. *Nature* **2008**, *452*, 580–589.
6. Louie, A. Multimodality Imaging Probes: Design and Challenges. *Chem. Rev.* **2010**, *110*, 3146–3195.
7. Kobayashi, H.; Koyama, Y.; Barrett, T.; Hama, Y.; Regino, C. A. S.; Shin, I. S.; Jang, B.-S.; Le, N.; Paik, C. H.; Choyke, P. L.; *et al.* Multimodal Nanoprobes for Radionuclide and Five-Color Near-Infrared Optical Lymphatic Imaging. *ACS Nano* **2007**, *1*, 258–264.
8. Abraham, S. A.; Edwards, K.; Karlsson, G.; MacIntosh, S.; Mayer, L. D.; McKenzie, C.; Bally, M. B. Formation of Transition Metal-Doxorubicin Complexes inside Liposomes. *Biochim. Biophys. Acta* **2002**, *1565*, 41–54.
9. Kim, B.-S.; Taton, T. A. Multicomponent Nanoparticles *via* Self-Assembly with Cross-Linked Block Copolymer Surfactants. *Langmuir* **2006**, *23*, 2198–2202.
10. Onuki, Y.; Jacobs, I.; Artemov, D.; Kato, Y. Noninvasive Visualization of *in Vivo* Release and Intratumoral Distribution of Surrogate MR Contrast Agent Using the Dual MR Contrast Technique. *Biomaterials* **2010**, *31*, 7132–7138.
11. Na, K.; Lee, S. A.; Jung, S. H.; Shin, B. C. Gadolinium-Based Cancer Therapeutic Liposomes for Chemotherapeutics and Diagnostics. *Colloids Surf., B* **2011**, *84*, 82–87.
12. Ghaghada, K.; Hawley, C.; Kawaji, K.; Annapragada, A.; Mukundan, S., Jr. T1 Relaxivity of Core-Encapsulated Gadolinium Liposomal Contrast Agents—Effect of Liposome Size and Internal Gadolinium Concentration. *Acad. Radiol.* **2008**, *15*, 1259–1263.
13. Kong, H. J.; Mooney, D. J. Microenvironmental Regulation of Biomacromolecular Therapies. *Nat. Rev. Drug Discovery* **2007**, *6*, 455–463.
14. Henrotte, V.; Laurent, S.; Gabelica, V.; Elst, L. V.; Depauw, E.; Muller, R. N. Investigation of Non-Covalent Interactions between Paramagnetic Complexes and Human Serum Albumin by Electrospray Mass Spectrometry. *Rapid Commun. Mass Spectrom.* **2004**, *18*, 1919–1924.
15. Wang, Y.; Spiller, M.; Caravan, P. Evidence for Weak Protein Binding of Commercial Extracellular Gadolinium Contrast Agents. *Magn. Reson. Med.* **2010**, *63*, 609–616.
16. Mulder, W. J. M.; Strijkers, G. J.; Griffioen, A. W.; van Bloois, L.; Molema, G.; Storm, G.; Koning, G. A.; Nicolay, K. A Liposomal System for Contrast-Enhanced Magnetic Resonance Imaging of Molecular Targets. *Bioconjugate Chem.* **2004**, *15*, 799–806.
17. Accardo, A.; Tesauro, D.; Roscigno, P.; Gianolio, E.; Paduano, L.; D'Errico, G.; Pedone, C.; Morelli, G. Physicochemical Properties of Mixed Micellar Aggregates Containing CCK Peptides and Gd Complexes Designed as Tumor Specific Contrast Agents in MRI. *J. Am. Chem. Soc.* **2004**, *126*, 3097–3107.
18. Gong, P.; Chen, Z.; Chen, Y.; Wang, W.; Wang, X.; Hu, A. High-Relaxivity MRI Contrast Agents Prepared from Miniemulsion Polymerization Using Gadolinium(III)-Based Metallosurfactants. *Chem. Commun.* **2011**, *47*, 4240–4242.
19. Ratzinger, G.; Agrawal, P.; Körner, W.; Lonkai, J.; Sanders, H. M. H. F.; Terreno, E.; Wirth, M.; Strijkers, G. J.; Nicolay, K.; Gabor, F. Surface Modification of PLGA Nanospheres with Gd-DTPA and Gd-DOTA for High-Relaxivity MRI Contrast Agents. *Biomaterials* **2010**, *31*, 8716–8723.
20. Liu, L.; Law, W.-C.; Yong, K.-T.; Roy, I.; Ding, H.; Erogbogbo, F.; Zhang, X.; Prasad, P. N. Multimodal Imaging Probes Based on Gd-DOTA Conjugated Quantum Dot Nanomicelles. *Analyst* **2011**, *136*, 1881–1886.
21. Kamaly, N.; Xiao, Z.; Valencia, P. M.; Radovic-Moreno, A. F.; Farokhzad, O. C. Targeted Polymeric Therapeutic Nanoparticles: Design, Development and Clinical Translation. *Chem. Soc. Rev.* **2012**, *41*, 2971–3010.
22. Singer, S. J.; Nicolson, G. L. The Fluid Mosaic Model of the Structure of Cell Membranes. *Science* **1972**, *175*, 720–731.
23. White, S. H. Membrane Protein Insertion: The Biology-Physics Nexus. *J. Cell Biol.* **2007**, *177*, 363–369.
24. Paulick, M. G.; Bertozzi, C. R. The Glycosylphosphatidylinositol Anchor: A Complex Membrane-Anchoring Structure for Proteins. *Biochemistry* **2008**, *47*, 6991–7000.
25. Guy-Caffey, J. K.; Webster, R. E. The Membrane Domain of a Bacteriophage Assembly Protein. Transmembrane-Directed Proteolysis of a Membrane-Spanning Fusion Protein. *J. Biol. Chem.* **1993**, *268*, 5488–95.
26. Gallusser, A.; Kuhn, A. Initial Steps in Protein Membrane Insertion. Bacteriophage M13 Procoat Protein Binds to the Membrane Surface by Electrostatic Interaction. *EMBO J.* **1990**, *9*, 2723–9.
27. Kuhn, A.; Kreil, G.; Wickner, W. Both Hydrophobic Domains of M13 Procoat Are Required To Initiate Membrane Insertion. *EMBO J.* **1986**, *5*, 3681–3685.
28. Ayyagari, A. L.; Zhang, X.; Ghaghada, K. B.; Annapragada, A.; Hu, X.; Bellamkonda, R. V. Long-Circulating Liposomal Contrast Agents for Magnetic Resonance Imaging. *Magn. Reson. Med.* **2006**, *55*, 1023–1029.
29. Yuan, H.; Lu, L.-J.; Du, Y.-Z.; Hu, F.-Q. Stearic Acid-g-Chitosan Polymeric Micelle for Oral Drug Delivery: *In Vitro* Transport and *in Vivo* Absorption. *Mol. Pharmaceutics* **2010**, *8*, 225–238.
30. Darras, V.; Nelea, M.; Winnik, F. M.; Buschmann, M. D. Chitosan Modified with Gadolinium Diethylenetriaminepentaacetic Acid for Magnetic Resonance Imaging of DNA/Chitosan Nanoparticles. *Carbohydr. Polym.* **2010**, *80*, 1137–1146.
31. Barge, A.; Cravotto, G.; Gianolio, E.; Fedeli, F. How to Determine Free Gd and Free Ligand in Solution of Gd Chelates. A Technical Note. *Contrast Media Mol. Imaging* **2006**, *1*, 184–188.
32. MicroCal, LLC. *ITC Data Analysis in Origin—Tutorial Guide*, 5th ed.; MicroCal LLC: Northampton, MA, 1998.
33. Israelachvili, J. N. Thermodynamic Principles of Self-Assembly. In *Intermolecular and Surface Forces*, 3rd ed.; Academic Press: San Diego, CA, 2011; pp 503−534.
34. Quemeneur, F.; Rinaudo, M.; Maret, G.; Pepin-Donat, B. Decoration of Lipid Vesicles by Polyelectrolytes: Mechanism and Structure. *Soft Matter* **2010**, *6*, 4471–4481.
35. Taira, M. C.; Chiaramoni, N. S.; Pecuch, K. M.; Alonso-Romanowski, S. Stability of Liposomal Formulations in Physiological Conditions for Oral Drug Delivery. *Drug Delivery* **2004**, *11*, 123–128.

36. Kirby, C.; Clarke, J.; Gregoriadis, G. Effect of the Cholesterol Content of Small Unilamellar Liposomes on Their Stability *In Vivo* and *in Vitro*. *Biochem. J.* **1980**, *186*, 591–598.
37. Limbourg, A.; Korff, T.; Napp, L. C.; Schaper, W.; Drexler, H.; Limbourg, F. P. Evaluation of Postnatal Arteriogenesis and Angiogenesis in a Mouse Model of Hind-Limb Ischemia. *Nat. Protocols* **2009**, *4*, 1737–1748.
38. Niiyama, H.; Huang, N. F.; Rollins, M. D.; Cooke, J. P. Murine Model of Hindlimb Ischemia. *J. Visualized Exp.* **2009**, 1035.
39. Hong, G.; Lee, J. C.; Robinson, J. T.; Raaz, U.; Xie, L.; Huang, N. F.; Cooke, J. P.; Dai, H. Multifunctional *in Vivo* Vascular Imaging Using Near-Infrared II Fluorescence. *Nat. Med.* **2012**, *18*, 1841–1846.
40. Dagher, P. C.; Herget-Rosenthal, S.; Ruehm, S. G.; Jo, S.-K.; Star, R. A.; Agarwal, R.; Molitoris, B. A. Newly Developed Techniques to Study and Diagnose Acute Renal Failure. *J. Am. Soc. Nephrol.* **2003**, *14*, 2188–2198.
41. Sarmento, B.; Mazzaglia, D.; Bonferoni, M. C.; Neto, A. P.; do Céu Monteiro, M.; Seabra, V. Effect of Chitosan Coating in Overcoming the Phagocytosis of Insulin Loaded Solid Lipid Nanoparticles by Mononuclear Phagocyte System. *Carbohydr. Polym.* **2011**, *84*, 919–925.
42. Amoozgar, Z.; Park, J.; Lin, Q.; Yeo, Y. Low Molecular-Weight Chitosan as a pH-Sensitive Stealth Coating for Tumor-Specific Drug Delivery. *Mol. Pharmaceutics* **2012**, *9*, 1262–1270.
43. Rohrer, M.; Bauer, H.; Mintorovitch, J.; Requardt, M.; Weinmann, H. J. Comparison of Magnetic Properties of MRI Contrast Media Solutions at Different Magnetic Field Strengths. *Invest. Radiol.* **2005**, *40*, 715–724.
44. Odintsov, B. Tunable Radiofrequency Coil. U.S. Patent US 8,049,502 B2, November 1, 2011.